

## The brightest gamma-ray flaring blazar in the sky: AGILE and multi-wavelength observations of 3C 454.3 during November 2010

S. Vercellone<sup>1</sup>, E. Striani<sup>2,3</sup>, V. Vittorini<sup>4</sup>, I. Donnarumma<sup>4</sup>, L. Pacciani<sup>4</sup>, G. Pucella<sup>5</sup>,  
M. Tavani<sup>2,3,4,6</sup>, C.M. Raiteri<sup>7</sup>, M. Villata<sup>7</sup>, P. Romano<sup>1</sup>, M. Fiocchi<sup>4</sup>, A. Bazzano<sup>4</sup>,  
V. Bianchin<sup>8</sup>, C. Ferrigno<sup>9</sup>, L. Maraschi<sup>10</sup>, E. Pian<sup>11,12,13</sup>, M. Türlér<sup>9</sup>, P. Ubertini<sup>4</sup>,  
A. Bulgarelli<sup>8</sup>, A.W. Chen<sup>14</sup>, A. Giuliani<sup>14</sup>, F. Longo<sup>15</sup>, G. Barbiellini<sup>15</sup>, M. Cardillo<sup>2,4</sup>,  
P.W. Cattaneo<sup>16</sup>, E. Del Monte<sup>4</sup>, Y. Evangelista<sup>4</sup>, M. Feroci<sup>4</sup>, A. Ferrari<sup>6,17</sup>, F. Fuschino<sup>8</sup>,  
F. Gianotti<sup>8</sup>, M. Giusti<sup>4</sup>, F. Lazzarotto<sup>4</sup>, A. Pellizzoni<sup>18</sup>, G. Piano<sup>4</sup>, M. Pilia<sup>18,19</sup>,  
M. Rapisarda<sup>5</sup>, A. Rappoldi<sup>16</sup>, S. Sabatini<sup>4</sup>, P. Soffitta<sup>4</sup>, M. Trifoglio<sup>8</sup>, A. Trois<sup>18</sup>,  
P. Giommi<sup>20</sup>, F. Lucarelli<sup>20</sup>, C. Pittori<sup>20</sup>, P. Santolamazza<sup>20</sup>, F. Verrecchia<sup>20</sup>, I. Agudo<sup>21,22</sup>,  
H.D. Aller<sup>23</sup>, M.F. Aller<sup>23</sup>, A.A. Arkharov<sup>24</sup>, U. Bach<sup>25</sup>, A. Berdyugin<sup>26</sup>, G.A. Borman<sup>27</sup>,  
R. Chigladze<sup>31</sup>, Yu.S. Efimov<sup>27</sup>, N.V. Efimova<sup>24,28</sup>, J.L. Gómez<sup>21</sup>, M.A. Gurwell<sup>29</sup>,  
I.M. McHardy<sup>30</sup>, M. Joshi<sup>22</sup>, G.N. Kimeridze<sup>31</sup>, T. Krajci<sup>32</sup>, O.M. Kurtanidze<sup>31</sup>,  
S.O. Kurtanidze<sup>31</sup>, V.M. Larionov<sup>24,28,33</sup>, E. Lindfors<sup>26</sup>, S.N. Molina<sup>21</sup>, D.A. Morozova<sup>28</sup>,  
S.V. Nazarov<sup>27</sup>, M.G. Nikolashvili<sup>31</sup>, K. Nilsson<sup>34</sup>, M. Pasanen<sup>26</sup>, R. Reinthal<sup>26</sup>, J.A. Ros<sup>35</sup>,  
A.C. Sadun<sup>36</sup>, T. Sakamoto<sup>37</sup>, S. Sallum<sup>38,39</sup>, S.G. Sergeev<sup>27</sup>, R.D. Schwartz<sup>40</sup>, L.A. Sigua<sup>31</sup>,  
A. Sillanpää<sup>26</sup>, K.V. Sokolovsky<sup>25</sup>, V. Strelitski<sup>38</sup>, L. Takalo<sup>26</sup>, B. Taylor<sup>22,41</sup>, G. Walker<sup>38</sup>

stefano.vercellone@iasf-palermo.inaf.it

---

<sup>1</sup>INAF/IASF–Palermo, Via U. La Malfa 153, I-90146 Palermo, Italy

- 
- <sup>2</sup>Dip. di Fisica, Univ. “Tor Vergata”, Via della Ricerca Scientifica 1, I-00133 Roma, Italy
- <sup>3</sup>INFN–Roma “Tor Vergata”, Via della Ricerca Scientifica 1, I-00133 Roma, Italy
- <sup>4</sup>INAF/IASF–Roma, Via del Fosso del Cavaliere 100, I-00133 Roma, Italy
- <sup>5</sup>ENEA–Frascati, Via E. Fermi 45, I-00044 Frascati (Roma), Italy
- <sup>6</sup>CIFS–Torino, Viale Settimio Severo 3, I-10133, Torino, Italy
- <sup>7</sup>INAF, Osservatorio Astronomico di Torino, Via Osservatorio 20, I-10025 Pino Torinese, Italy
- <sup>8</sup>INAF/IASF–Bologna, Via Gobetti 101, I-40129 Bologna, Italy
- <sup>9</sup>ISDC, Université de Genève, chemin d’Écogia, 16 1290 Versoix Switzerland
- <sup>10</sup>INAF, Osservatorio Astronomico di Brera, via E. Bianchi 46, 23807, Merate, Italy
- <sup>11</sup>INAF, Osservatorio Astronomico di Trieste, Via G.B. Tiepolo 11, 34143 Trieste, Italy
- <sup>12</sup>Scuola Normale Superiore, Piazza dei Cavalieri 7, 56126 Pisa, Italy
- <sup>13</sup>ESO, Karl-Schwarzschild-Strasse 2, 85748 Garching bei München, Germany
- <sup>14</sup>INAF/IASF–Milano, Via E. Bassini 15, I-20133 Milano, Italy
- <sup>15</sup>Dip. di Fisica and INFN, Via Valerio 2, I-34127 Trieste, Italy
- <sup>16</sup>INFN–Pavia, Via Bassi 6, I-27100 Pavia, Italy
- <sup>17</sup>Dip. di Fisica Generale, Univ. degli Studi di Torino, via P. Giuria 1, I-10125 Torino, Italy
- <sup>18</sup>INAF, Osservatorio Astronomico di Cagliari, località Poggio dei Pini, strada 54, I-09012 Capoterra, Italy
- <sup>19</sup>Dip. di Fisica, Univ. degli Studi dell’Insubria, via Valleggio 11, I-22100, Como, Italy
- <sup>20</sup>ASI–ASDC, Via G. Galilei, I-00044 Frascati (Roma), Italy
- <sup>21</sup>Instituto de Astrofísica de Andalucía, CSIC, Apartado 3004, 18080, Granada, Spain
- <sup>22</sup>Institute for Astrophysical Research, Boston University, 725 Commonwealth Avenue, Boston, MA 02215, USA
- <sup>23</sup>Department of Astronomy, University of Michigan, MI, USA
- <sup>24</sup>Pulkovo Observatory St.-Petersburg, Russia
- <sup>25</sup>Max-Planck-Institut für Radioastronomie, Auf dem Hügel 69, 53121 Bonn, Germany
- <sup>26</sup>Tuorla Observatory, University of Turku, FIN-21500 Piikkiö, Finland
- <sup>27</sup>Crimean Astrophysical Observatory, 98049 Nauchny, Crimea, Ukraine
- <sup>28</sup>Astronomical Institute, St.-Petersburg State University, Russia
- <sup>29</sup>Harvard-Smithsonian Center for Astrophysics, MA, USA
- <sup>30</sup>Department of Physics and Astronomy, University of Southampton, Southampton, SO17 1BJ, United

## ABSTRACT

Since 2005, the blazar 3C 454.3 has shown remarkable flaring activity at all frequencies, and during the last four years it has exhibited more than one  $\gamma$ -ray flare per year, becoming the most active  $\gamma$ -ray blazar in the sky. We present for the first time the multi-wavelength AGILE, *Swift*, INTEGRAL, and GASP-WEBT data collected in order to explain the extraordinary  $\gamma$ -ray flare of 3C 454.3 which occurred in November 2010. On 2010 November 20 (MJD 55520), 3C 454.3 reached a peak flux ( $E > 100$  MeV) of  $F_{\gamma}^p = (6.8 \pm 1.0) \times 10^{-5}$  photons  $\text{cm}^{-2} \text{s}^{-1}$  on a time scale of about 12 hours, more than a factor of 6 higher than the flux of the brightest steady  $\gamma$ -ray source, the Vela pulsar, and more than a factor of 3 brighter than its previous super-flare on 2009 December 2–3. The multi-wavelength data make a thorough study of the present event possible: the comparison with the previous outbursts indicates a close similarity to the one that occurred in 2009. By comparing the broadband emission before, during, and after the  $\gamma$ -ray flare, we find that the radio, optical and X-ray emission varies within a factor 2–3, whereas the  $\gamma$ -ray flux by a factor of 10. This remarkable behavior is modeled by an external Compton component driven by a substantial local enhancement of soft seed photons.

*Subject headings:* galaxies: active – galaxies: quasars: general – galaxies: quasars: individual: 3C 454.3 – galaxies: jets – radiation mechanism: non thermal

---

Kingdom

<sup>31</sup>Abastumani Observatory, Mt. Kanobili, 0301 Abastumani, Georgia

<sup>32</sup>Astrokolkhov Observatory, P.O. Box 1351, Cloudcroft, NM 88317, USA

<sup>33</sup>Isaac Newton Institute of Chile, St.-Petersburg Branch, Russia

<sup>34</sup>Finnish Centre for Astronomy with ESO (FINCA), University of Turku, FIN-21500 Piikkiö, Finland

<sup>35</sup>Agrupació Astronòmica de Sabadell, Spain

<sup>36</sup>Department of Physics, University of Colorado Denver, CO, USA

<sup>37</sup>Center for Research and Exploration in Space Science and Technology, NASA/GSFC, Greenbelt, MD, USA

<sup>38</sup>Maria Mitchell Observatory, Nantucket, MA 02554

<sup>39</sup>Massachusetts Institute of Technology, 77 Massachusetts

<sup>40</sup>Galaxy View Observatory, 102 Galaxy View Ct. Sequim, Washington 98382, USA

<sup>41</sup>Lowell Observatory, Flagstaff, AZ 86001, USA

## 1. Introduction

The flat spectrum radio quasar 3C 454.3 (PKS 2251+158;  $z = 0.859$ ) is the brightest  $\gamma$ -ray (0.1–10 GeV) blazar detected after the launch of the AGILE (Tavani et al. 2009) and *Fermi* (Atwood et al. 2009) satellites. During 2007 – 2010, AGILE detected and investigated several gamma-ray flares (Vercellone et al. 2010a; Pacciani et al. 2010; Striani et al. 2010d). These observations allowed us to establish a possible correlation between the  $\gamma$ -ray (0.1 – 10 GeV) and the optical (R band) flux variations with no time delay, or with a lag of the former with respect to the latter of about half a day. Moreover, the detailed physical modeling of the spectral energy distributions (SEDs) when 3C 454.3 was at different flux levels provided an interpretation of the emission mechanism responsible for the radiation emitted in the  $\gamma$ -ray energy band, assumed to be inverse Compton scattering of photons from the broad line region (BLR) clouds off the relativistic electrons in the jet, with bulk Lorentz factor  $\Gamma \sim 20$ . Similar results were obtained by other groups, by analyzing *Fermi* and multi-wavelength data (e.g., Ghisellini et al. 2007; Bonning et al. 2009; Abdo et al. 2009; Foschini et al. 2010; Bonnoli et al. 2011). During the period 2009 December 2–3, 3C 454.3 exhibited an intense  $\gamma$ -ray flare reaching a peak value of  $F_{\gamma}^{\text{p},2009} = (2.0 \pm 0.4) \times 10^{-5} \text{ photons cm}^{-2} \text{ s}^{-1}$  in the range 0.1–10 GeV. This extreme behavior in the  $\gamma$ -ray might require a more sophisticated modeling with respect to the widely accepted one-zone, synchrotron self-Compton (SSC) and external Compton (EC) models (Celotti & Ghisellini 2008, for a review of the blazar emission mechanisms and energetics). In particular, the almost simultaneous multi-wavelength data collected during the  $\gamma$ -ray flare required an additional population of accelerated electrons co-existing with the soft seed photons of the SSC/EC model (Pacciani et al. 2010). Alternatively to the SSC/EC models, the blazar SED can be explained in the framework of the hadronic models (Mannheim & Schlickeiser 1994; Mücke & Protheroe 2001; Becker 2008).

Recently, Foschini et al. (2011) and Abdo et al. (2011), analyzing *Fermi* data acquired during the November 2010 flare, show that the extremely fast variability, on a time-scale of about 3–6 hr, favors a  $\gamma$ -ray emission originating from a compact region, below the pc scale.

In this Letter we report on the multi-wavelength AGILE, *Swift*, INTEGRAL, and GASP-WEBT campaign covering the extraordinary November 2010  $\gamma$ -ray flare of 3C 454.3. The quoted uncertainties are given at the  $1\sigma$  level, unless otherwise stated, and a  $\Lambda$ -CDM cosmology ( $h = 0.71$ ,  $\Omega_m = 0.27$ , and  $\Omega_{\Lambda} = 0.73$ ) was adopted.

## 2. Data Analysis

AGILE detected increased and prolonged  $\gamma$ -ray emission from 3C 454.3 starting from 2010 October 28 (MJD 55497), with a maximum emission on 2010 November 20 (MJD 55520, Vercellone et al. 2010b; Striani et al. 2010a,b,c). Level-1 AGILE-GRID data were analyzed using the AGILE Standard Analysis Pipeline (see Vercellone et al. 2010a, for a description of the AGILE data reduction). We used  $\gamma$ -ray events filtered with the **FM3.119** AGILE Filter pipeline. Counts, exposure, and Galactic background  $\gamma$ -ray maps were created with a bin-size of  $0.5^\circ \times 0.5^\circ$ ,  $E \geq 100$  MeV, and including all events collected up to  $60^\circ$  off-axis. To reduce the  $\gamma$ -ray Earth albedo contamination, we rejected all  $\gamma$ -ray events whose reconstructed directions form angles with the satellite-Earth vector  $< 85^\circ$ . We used the latest version (**BUILD-20**) of the Calibration files (**I0010**), which will be publicly available at the ASI Science Data Centre (ASDC) site<sup>1</sup>, and of the  $\gamma$ -ray diffuse emission model (Giuliani et al. 2004). We ran the AGILE Multi-Source Maximum Likelihood Analysis (**ALIKE**) task with an analysis radius of  $10^\circ$ .

The *Swift* X-ray Telescope (XRT) data were processed with standard procedures (XRT-PIPELINE v0.12.6 within HEASOFT V.6.10), filtering and screening criteria. The XRT data were in windowed timing mode (WT). Spectra were extracted on an orbit-by-orbit basis due to a rotation of the roll angle, within circular regions with a radius of 47.15 arcsec. We used the latest spectral redistribution matrices (20101206). The *Swift* Ultraviolet and Optical Telescope (UVOT) data analysis was performed using the **uvotimsum** and **uvotsource** tasks. Source counts were extracted from a circular region with a 5 arcsec radius. The background was extracted from a nearby source-free circular regions. The reported fluxes are on the UVOT photometric system described in Poole et al. (2008), and are not corrected for Galactic extinction.

The INTEGRAL data were obtained as a Target of Opportunity (ToO) observation triggered immediately after the  $\gamma$ -ray flare (for preliminary results see Pian et al. 2010), and were processed using the ISDC Off-line Scientific Analysis software (**OSA V.9.0**, Courvoisier et al. 2003). INTEGRAL observed the source between 2010 November 21.70 UT and November 27.24 UT, for a total on source time of 400 ks. Light curves and spectra were extracted for each individual science window (SCW) and later combined. We investigated the 4 – 26 keV (JEM-X both units) and 20 – 200 keV (IBIS/ISGRI) energy ranges. We extracted the light-curve from IBIS/ISGRI in the 20–40 keV, and 40–100 keV energy bands to verify possible variability on time scales from hours to one day: the average count rate in the softer (harder) band is  $1.6 \pm 0.1$  counts s<sup>−1</sup> ( $1.4 \pm 0.1$  counts s<sup>−1</sup>), or about 11 (15) mCrab without significant

---

<sup>1</sup><http://agile.asdc.asi.it>

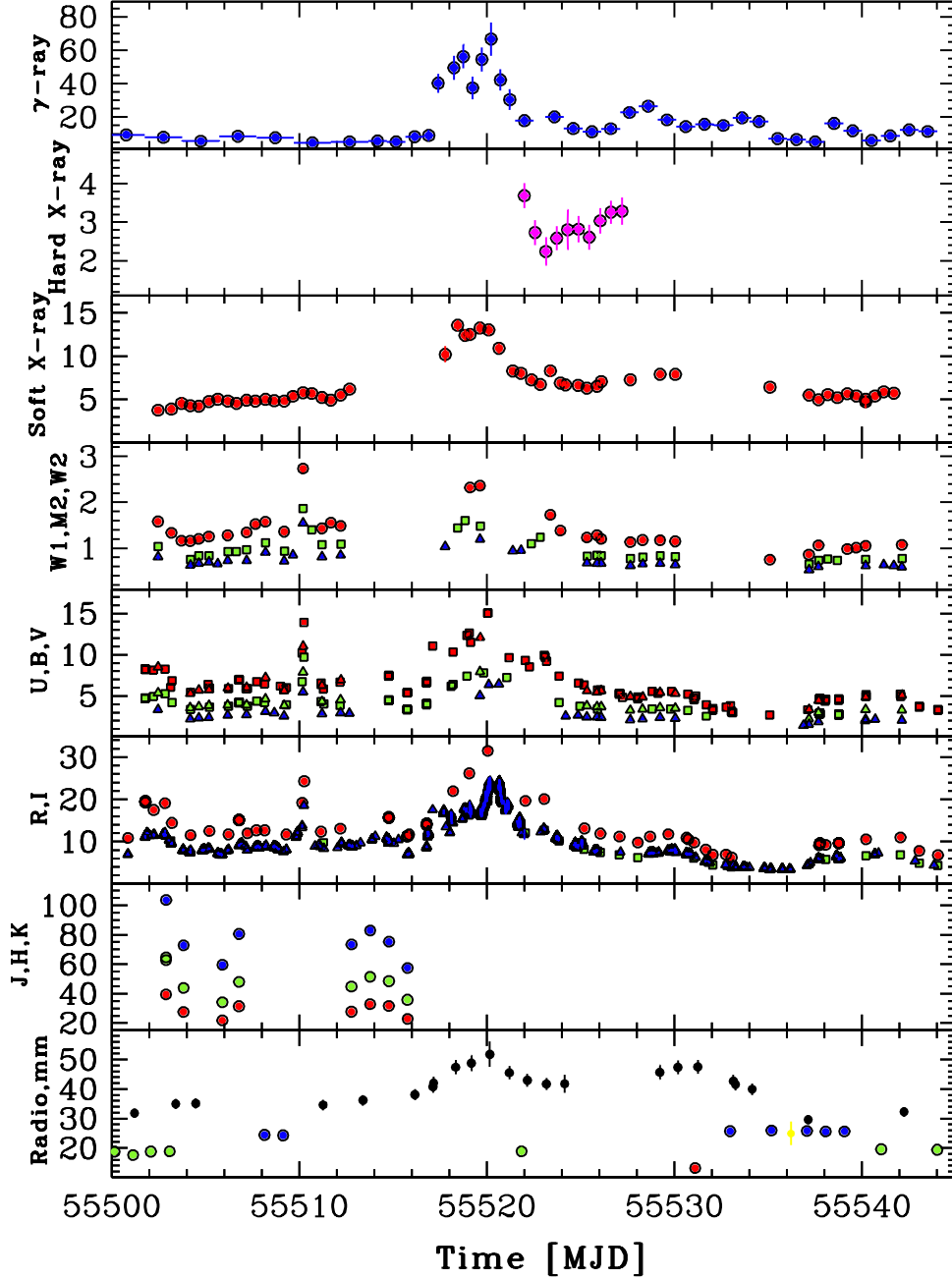


Fig. 1.— Multi-wavelength light curves from radio to  $\gamma$ -ray.  $\gamma$ -ray ( $E > 100$  MeV) data are in units of  $10^{-6}$  photons  $\text{cm}^{-2} \text{s}^{-1}$ ; hard X-ray (20–100 keV) data are in units of counts  $\text{s}^{-1}$ ; soft X-ray (2–10 keV) data are in units of  $10^{-11}$  erg  $\text{cm}^{-2} \text{s}^{-1}$ ; UV, optical and NIR data are in units of mJy; radio data are in units of Jy. See § 3 for details. The starting date, MJD 55500, corresponds to 2010-10-31 00:00 UT.

variability. We then analyzed the averaged spectrum using 8 pre-defined energy channels in JEM-X and 16 customized energy channels for IBIS/ISGRI with XSPEC (v. 12.6.0). We assumed a single power law model and free cross-calibration constants for JEM-X ( $C_1$  and  $C_2$ ) with respect to ISGRI, and a 3% systematic error to account for the instrumental calibration uncertainties. We obtain (uncertainties at 90% c.l.):  $\Gamma = 1.59 \pm 0.08$  ( $\chi^2_{\text{red}}/\text{d.o.f.} = 1.35/23$ ),  $C_1 = 1.1 \pm 0.2$ ,  $C_2 = 1.3 \pm 0.2$ ,  $F_{4-200 \text{ keV}} = (4.7^{+0.2}_{-0.4}) \times 10^{-10} \text{ erg cm}^{-2} \text{ s}^{-1}$ .

The GLAST-AGILE Support Program (GASP; Villata et al. 2008, 2009) is a project born from the Whole Earth Blazar Telescope<sup>2</sup> (WEBT) in 2007, which has analysed the multi-frequency behavior of 3C 454.3 since the unprecedented optical outburst of 2005 (Villata et al. 2006, 2007; Raiteri et al. 2007, 2008a,b; Villata et al. 2009; Raiteri et al. 2011). The *R*-band GASP observations of 3C 454.3 in the period considered in this paper were performed by the following observatories: Abastumani, Calar Alto, Crimean, Galaxy View, Goddard (GRT), Lowell (Perkins), Maria Mitchell, New Mexico Skies, ROVOR, Roque de los Muchachos (KVA and Liverpool), Sabadell, and St. Petersburg. Additional data were taken by the AAVSO<sup>3</sup> (Krajci et al. 2010) and the Yale Fermi/SMARTS project<sup>4</sup> (Chatterjee et al. 2011). Some of the above observatories also provided data in the *B*, *V*, and *I* bands. Near-IR (NIR) data in *J*, *H*, and *K* bands are from Campo Imperatore. Radio flux densities were measured at: Submillimeter Array (SMA, 345 and 230 GHz, see Gurwell et al. 2007), Medicina (8 GHz), and UMRAO (14.5, 8.0, and 4.8 GHz). Data reduction and analysis follow Raiteri et al. (2008a).

### 3. Results

Figure 1 shows the multi-wavelength light curves from radio to  $\gamma$ -ray; from top to bottom: AGILE/GRID ( $E > 100$  MeV) at a variable time-bin of  $\approx 2, 1$ , and  $0.5$ -day; INTEGRAL (20–100 keV); *Swift*/XRT (2–10 keV); *Swift*/UVOT UV *w1* (red circles), *m2* (green squares), and *w2* (blue triangles); *Swift*/UVOT (triangles), and GASP-WEBT (squares) optical *U* (blue points), *B* (green points), and *V* (red points); GASP-WEBT optical *R* (blue triangles, with additional data from AAVSO as green squares) and *I* (red circles); GASP-WEBT near infra-red *J* (red points), *H* (green points), and *K* (blue points); and GASP-WEBT 4.8 GHz (red circles), 8 GHz (green circles), 14.5 GHz (blue circles), 230 GHz (black circles), and 345 GHz (yellow circles).

---

<sup>2</sup><http://www.oato.inaf.it/blazars/webt/>

<sup>3</sup><http://www.aavso.org/>

<sup>4</sup><http://www.astro.yale.edu/smarts/glast/>

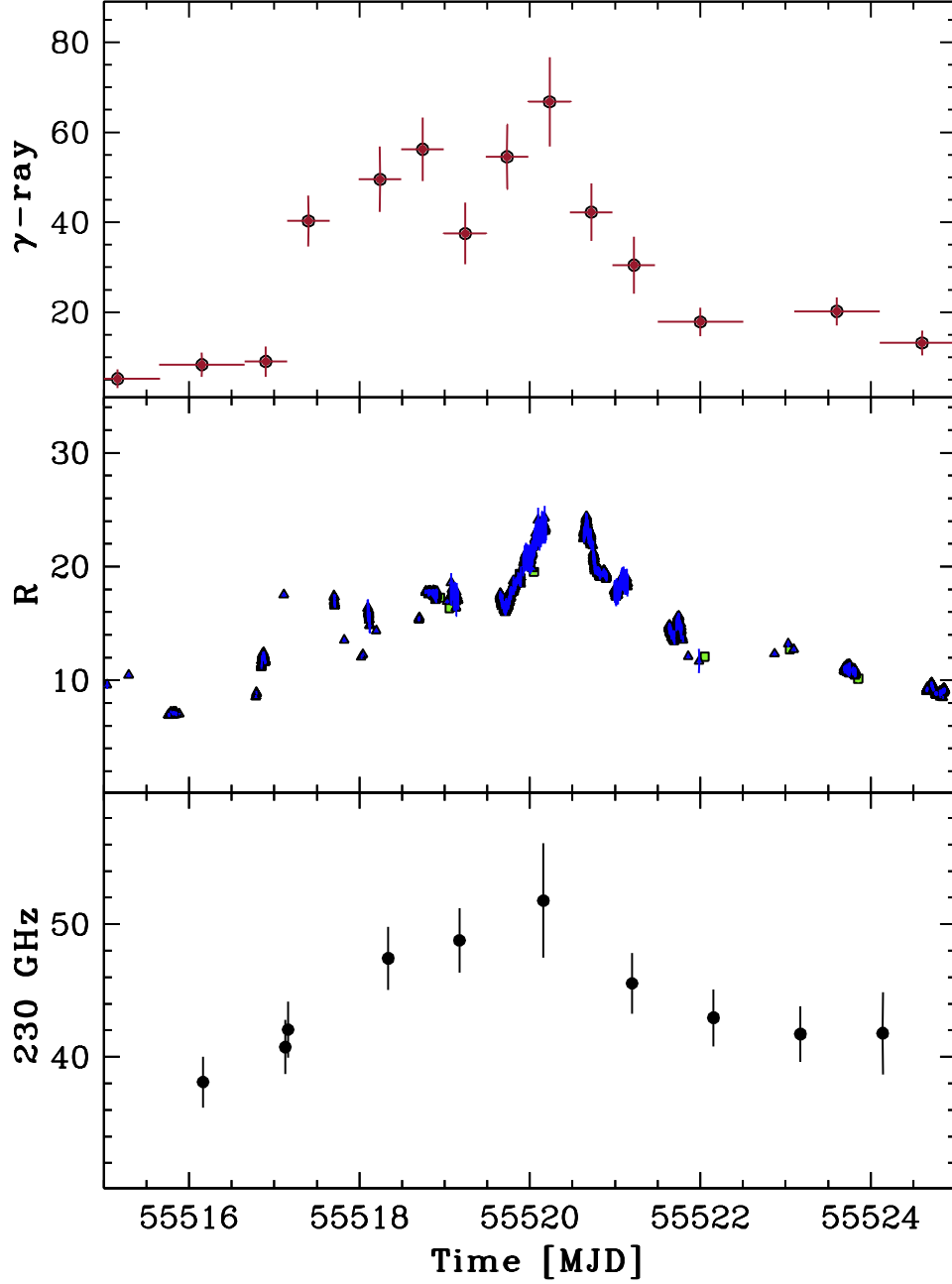


Fig. 2.— Zoom of the  $\gamma$ -ray (top panel),  $R$ -band (middle panel), and 230 GHz (bottom panel) light curves. Units and energy bands are the same as in Figure 1. The starting date, MJD 55515, corresponds to 2010-11-15 00:00 UT.



When data are available, a clear peak is present at approximately MJD 55520 in all light curves. In particular, the  $\gamma$ -ray light curve shows different behavior during the pre- and the post-flare periods, the former being much steadier than the latter, on almost the same time-scale. The UV and optical light curves show a very similar trend, in particular the remarkably fast flare centered at approximately MJD 55510, with rising and falling of about a factor of 2–2.5 in about 48 hours. During the same period, the X-ray flux varied by about 20%, while no significant variability is detected at other wavelengths. We also note that there is an average offset between the GASP-WEBT and *Swift*/UVOT data in the  $V$  and  $B$  band. If  $(V, B)$  and  $(v, b)$  are the GASP-WEBT and *Swift*/UVOT data, respectively, then a good agreement is found when  $B - b = 0.1$  mag, and  $V - v = -0.05$  mag. Raiteri et al. (2011) discuss the nature of this offset and provide a tool for the calibration of the *Swift*/UVOT data. Figure 2 shows a zoom, centered on the  $\gamma$ -ray flare date, of the  $\gamma$ -ray,  $R$ -band and 230 GHz light curves. We note that, to the sudden enhancement (about a factor of 4) of the gamma-ray flux on MJD 55517, does not correspond a similar flare in the other wavebands.

The *Swift*/XRT spectra were rebinned to have at least 20 counts per energy bin, and were fit with an absorbed power law model. Following Vercellone et al. (2010a), the Galactic absorption was fixed to the value of  $N_{\text{H}}^{\text{Gal}} = 1.34 \times 10^{21} \text{ cm}^{-2}$  (Villata et al. 2006). In Figure 3 (a), we show the X-ray photon index as a function of the 2–10 keV X-ray flux. No particular trend is present, contrary to what was previously reported in Vercellone et al. (2010a) for the period 2007–2009.

The  $\gamma$ -ray spectra were computed in four different time periods, pre-flare (MJD 55497.60 – 55516.40), flare (MJD 55518.25 – 55520.25), post-flare (MJD 55521.25 – 55543.75) and whole period. Table 1 shows the spectral parameters that we obtained by fitting the AGILE data with a simple power-law:

$$F(E) = k \times \left( \frac{E}{1 \text{ MeV}} \right)^{-\alpha}. \quad (1)$$

Table 1 reports the numerical values during the different time periods. We note that the flux during the flare is about a factor of 25 larger than the average value reported in the First AGILE Catalogue (Pittori et al. 2009, July 2007 - June 2008).

#### 4. Discussion

Since its launch in 2007, AGILE detected significant  $\gamma$ -ray emission from 3C 454.3 with repeated and prolonged flaring activity. Figure 3 (b), shows the ratio  $F_{\text{high}}^{\gamma}/F_{\text{low}}^{\gamma}$  as a function of time, where  $F_{\text{high}}^{\gamma}$  is the flux maximum value during each flare detected by AGILE, and

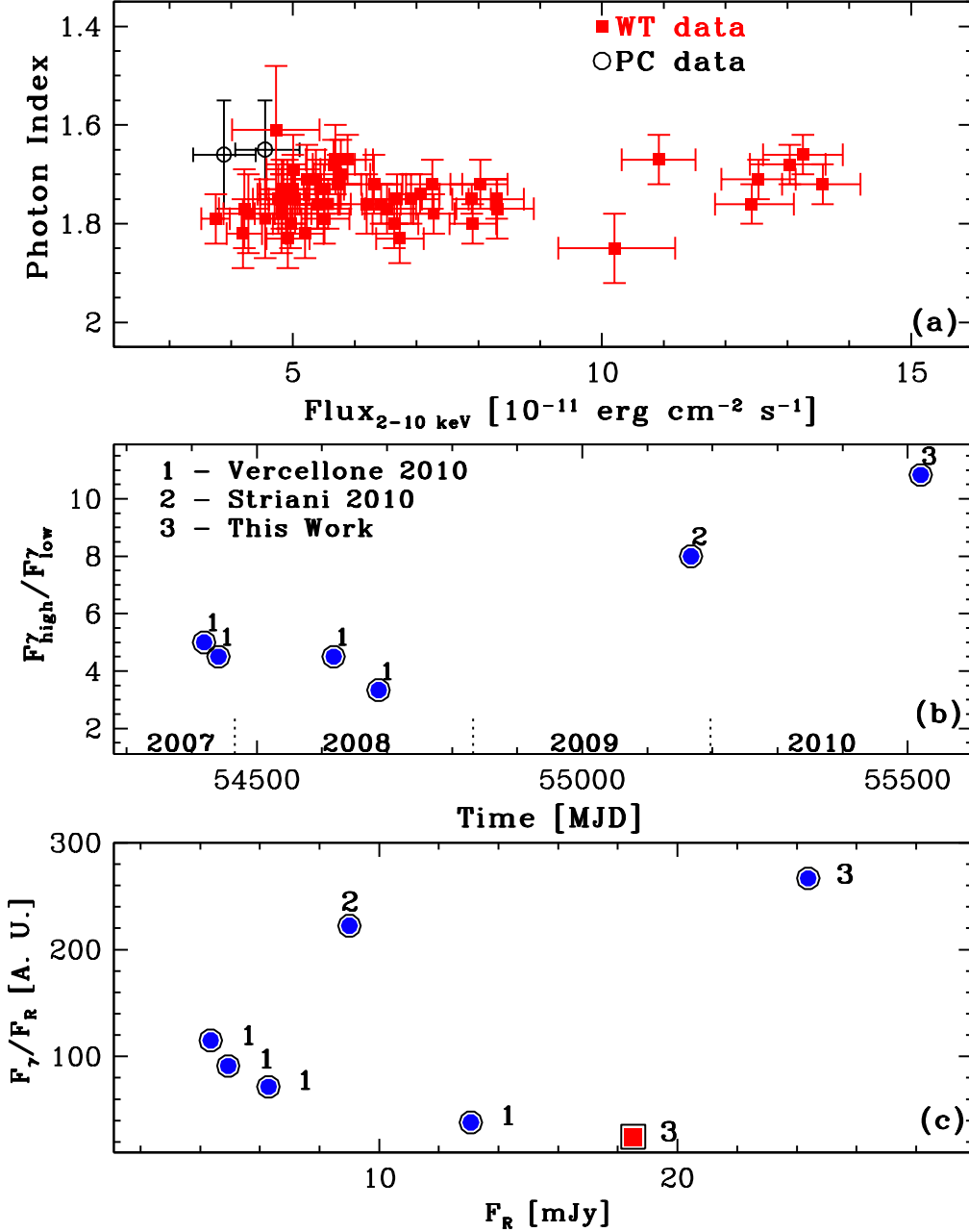


Fig. 3.— *Panel (a)*: X-ray photon index as a function of the X-ray flux in the energy band 2–10 keV. *Panel (b)*: peak over low  $\gamma$ -ray flux ratio for the major AGILE detected flares as a function of time. *Panel (c)*: blue circles represent the ratio between the  $\gamma$ -ray and  $R$ -band peak fluxes as a function of the  $R$ -band peak flux, while red square represents the same quantity for the fast optical–UV flare on MJD 55510.

$F_{\text{low}}^{\gamma}$  is the lowest flux point just before the corresponding rising in the light curve. While in 2007–2008 this ratio is of the order of 3–5, in 2009 and 2010 this ratio is at least a factor of 2–3 larger. It is worth noting that, during this latest flare, the 230 GHz, optical-UV, X-ray, and  $\gamma$ -ray flux variations are almost simultaneous. The 230 GHz flux shows a more prolonged active state after the  $\gamma$ -ray super-flare ( $\sim 10$  days), while the UV and optical fluxes reach levels comparable or lower than the pre-flare ones. The extremely large  $\gamma$ -ray dynamic range in the 2010 flare, the high 230 GHz flux level, and the relatively bright state in the optical band, when compared with other  $\gamma$ -ray flares, could not be explained only in terms of the alignment of different regions of the jet as suggested in Vercellone et al. (2010a). Figure 3 (c), provides further evidence of the different behavior of the 2009 and 2010 flares with respect to the previous ones. The plot of the ratio between the  $\gamma$ -ray and  $R$ -band peak fluxes as a function of the  $R$ -band peak flux (blue circles) shows a difference among flares in the different epochs.

The red square represents the point relative to the fast optical–UV flare on MJD 55510. This last point is particularly interesting because of the fast rising and decay time scales ( $\sim 1$  d). To explain the lack of a simultaneous  $\gamma$ -ray flare, a magnetic field enhancement by a factor of 2, a local  $\gamma$ - $\gamma$  absorption, or a locally seed-photon starved zone are required.

The INTEGRAL 20–100 keV light curve shows another peculiarity of the November 2010 flare with respect to the intense optical and X-ray flare of May 2005. During the November 2010 flare, the source shows only moderate flux variability ( $\approx 1.6\sigma$  level) and a relatively hard spectrum ( $\Gamma = 1.59 \pm 0.08$ ), while in 2005, during a comparably long observation at a comparable flux level, the source exhibited remarkable flux variability and a softer spectrum ( $\Gamma = 1.8 \pm 0.1$ , Pian et al. 2006). Despite the moderate variability in the 20–100 keV band, Figure 1 seems to show a similar trend between the light curves in the soft, hard X-ray and  $\gamma$ -ray bands.

Figure 4 shows SEDs chosen at three epochs with the largest number of data points. The NIR, optical, UV, and X-ray data are corrected for Galactic extinction. Green open triangles represent the pre-flare SED, accumulated on MJD 55512. In order to obtain enough statistics, the AGILE data were acquired in the period MJD 55497.60 – 55516.40. Red filled circles represent the flare SED, accumulated on MJD 55519 (AGILE data: MJD 55518.25 – 55520.25). Blue open squares represent the post-flare SED, accumulated on MJD 55526 (AGILE data: 55521.25 – 55543.75). The INTEGRAL IBIS/ISGRI integrated spectrum (MJD 55521.70 – 55527.30) is also reported.

We fit the pre-flare SED by means of a one-zone leptonic model, considering the contributions from SSC and from external seed photons originating both from the accretion disk (AD) and from the BLR (detailed description of this model is given in Vittorini et al. 2009).

Table 1. *Top:*  $\gamma$ -ray spectral parameters. *Bottom:* parameters for the pre-flare and flare, SED models, respectively (see § 4 for details).

Parameter	Pre-flare	Flare	Post-flare	Whole period	Units
$\gamma$ -ray spectral parameters					
$F_{E>100\text{ MeV}}$	$6.2 \pm 0.6$	$53.5 \pm 3.7$	$13.8 \pm 0.6$	$16.8 \pm 0.7$	$10^{-6} \text{ ph cm}^{-2} \text{ s}^{-1}$
$k$	0.4	11.1	10.0	3.8	$10^{-3} \text{ ph cm}^{-2} \text{ s}^{-1} \text{ MeV}^{-1}$
$\alpha$	$1.93 \pm 0.20$	$2.13 \pm 0.13$	$2.37 \pm 0.08$	$2.15 \pm 0.08$	
SEDs model parameters					
$\alpha_l$	2.35	2.35			
$\alpha_h$	4.2	4.8			
$\gamma_{\min}$	50	80			
$\gamma_b$	650	700			
$K$	300	700			$\text{cm}^{-3}$
$R_{blob}$	7.0	3.6			$10^{16} \text{ cm}$
$B$	0.65	1.1			G
$\delta$	34.5	34.5			
$L_d$	2	2			$10^{46} \text{ erg s}^{-1}$
$T_d$	$10^4$	$10^4$			$^{\circ}K$
$r_d$	0.05	0.05			pc
$\Theta_0$	1.15	1.15			degrees
$\Gamma$	20	20			

Indeed, emission from both the BLR and the AD were detected during faint states of the source (Raiteri et al. 2007). The solid lines represent the total contributions before (green), during (red), and after the flare (blue).

Hadronic models are challenged by the detection of correlated variability at different wavelength, as pointed out by Finke & Dermer (2010), and as observed by both *Fermi* and AGILE (but see Barkov et al. 2010).

The emission along the jet is assumed to be produced in a spherical blob with comoving radius  $R_{\text{blob}}$  by accelerated electrons characterized by a comoving broken power law energy density distribution,

$$n_e(\gamma) = \frac{K\gamma_b^{-1}}{(\gamma/\gamma_b)^{\alpha_l} + (\gamma/\gamma_b)^{\alpha_h}}, \quad (2)$$

where  $\gamma$  is the electron Lorentz factor varying between  $80 < \gamma < 8 \times 10^3$ ,  $\alpha_l$  and  $\alpha_h$  are the pre- and post-break electron distribution spectral indices, respectively, and  $\gamma_b$  is the break energy Lorentz factor. We assume that the blob contains an homogeneous and random magnetic field  $B$  and that it moves with a bulk Lorentz Factor  $\Gamma$  at an angle  $\Theta_0$  with respect to the line of sight. The relativistic Doppler factor is  $\delta = [\Gamma(1 - \beta \cos \Theta_0)]^{-1}$ , where  $\beta$  is the blob bulk speed in units of the speed of light. Our fit parameters are listed in Table 1.

Our modeling of the 3C 454.3 high-energy emission is based on an inverse Compton (IC) model with two main sources of external seed photons: (1) the AD characterized by a blackbody spectrum peaking in the UV with a bolometric luminosity  $L_d$  for an IC-scattering blob at a distance  $r_d$  from the central part of the disk<sup>5</sup>; (2) the BLR with a spectrum peaking in the V, placed at a distance from the central black hole of  $r_{\text{BLR}} = 3 \times 10^{18}$  cm, and assumed to reprocess 10% of the irradiating continuum (see Vercellone et al. 2009 for the first application of this model to 3C 454.3, and Pacciani et al. 2010 for the December 2009 flare modeling).

The flaring behavior in the optical and  $\gamma$ -ray energy bands is puzzling. We observe a first rapid flare at MJD 55510 with the optical flux rising and falling by a factor 2 in about 24 hours without a  $\gamma$ -ray counterpart. After a time  $T=7$  d, at MJD 55517, the optical flux increases by a factor of 2, followed after about 12 hours by a  $\gamma$ -ray increase by a factor of 4. On the contrary, on MJD 55520, the flux variations in the optical and  $\gamma$ -ray bands are of the same magnitude, as expected from an EC mechanism. This complex behavior challenges the idea of a uniform external photon field. A possible explanation is that an energetic particle

---

<sup>5</sup>We find  $r_d = 0.05$  pc, to be compared with  $r_s = 1.5 \times 10^{14}$  cm (assuming  $M_{\text{BH}} = 5 \times 10^8 M_\odot$ , Bonoli et al. 2011). Our distance value may challenge models in which the dissipation region distance is  $>$  a few pc (e.g., Jorstad et al. 2010).

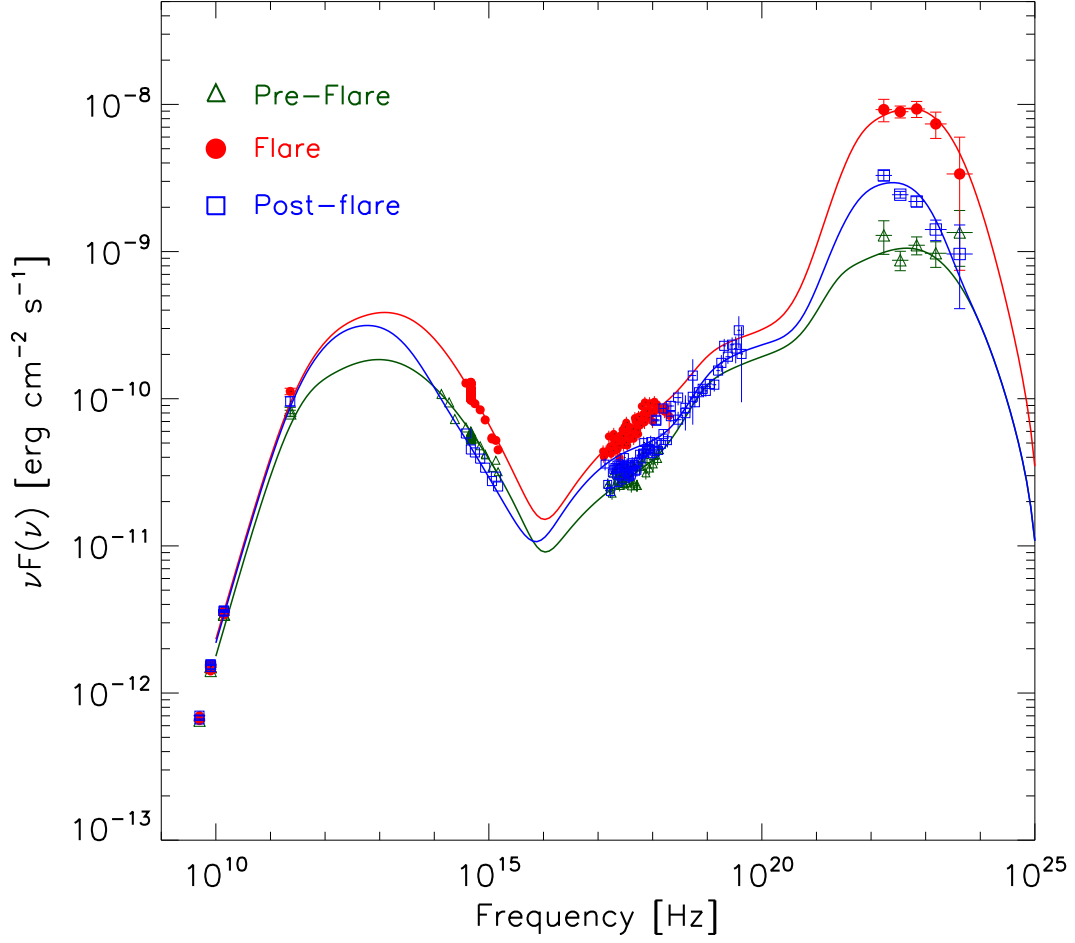


Fig. 4.— SEDs constructed before (green open triangles), during (red filled circles), and after (blue open squares) the flare. The NIR, optical, UV, and X-ray data are corrected for Galactic extinction. The fit lines and model parameters are described in § 4 and in Table 1.

ignition, taking place in an average-density photon region, causes the first optical flare at MJD 55510. Subsequently, the blob moves away by  $cT\delta/(1+z) \approx 3.4 \times 10^{17}$  cm towards a region with a denser external photon field in which a doubling in the optical flux can be followed by a stronger EC counterpart, as observed during the  $\gamma$ -ray enhanced emission at MJD 55517. Thereon, since the blob is moving in a region with enhanced density of external seed photons, the optical and  $\gamma$ -ray flux variations have similar dynamic range (as observed at MJD 55520), until the blob leaves this denser region. Alternatively, to explain the whole behavior, we can invoke a modest variation of  $\Gamma$ . Subsequently, as observed in the post-flare SED, the  $\gamma$ -ray emission decreases because of 1) the radiative cooling, and 2) the decrease of the external photon field due to the blob escaping the enhanced density region. The post-flare SED parameters, therefore, are similar to the flare ones, once evolution by radiative cooling is taken into account. During the flare, the total power carried in the jet,  $P_{\text{jet}}$ , defined as

$$P_{\text{jet}} = L_B + L_p + L_e + L_{\text{rad}} \text{ erg s}^{-1}, \quad (3)$$

(see also Ghisellini & Celotti 2001) where  $L_B$ ,  $L_p$ ,  $L_e$ , and  $L_{\text{rad}}$  are the power carried by the magnetic field, the cold protons<sup>6</sup>, the relativistic electrons, and the produced radiation, respectively, is of the order of  $P_{\text{jet}} \approx 10^{47}$  erg s<sup>-1</sup>.

We can now discuss the absence of a harder-when-brighter trend in the 2–10 keV energy band. During the 18-months AGILE campaign, Vercellone et al. (2010a) found a clear trend, in particular for fluxes above  $(1\text{--}2) \times 10^{-11}$  erg cm<sup>-2</sup> s<sup>-1</sup>. Donnarumma et al. (2010) show that a behavior similar to the November 2010 one was already present during the 2009 December 2–3  $\gamma$ -ray flare (see also Pacciani et al. 2010). We can describe the harder-when-brighter trend in terms of a dominant contribution of the EC off the disk seed photons, EC(Disk), over the SSC component, probably due to an increase of the accretion rate. We note that an increase of  $n_e$  and/or  $\gamma_b$  would cause a softer-when-brighter trend, inconsistent with our findings. The constant X-ray photon index during the extreme  $\gamma$ -ray flares in 2009 and 2010 can be interpreted in terms of a balance of the SSC contribution with respect to the EC(Disk). If we assume that  $\gamma_b$  increases significantly with respect to the 2007–2008 ones ( $\gamma_b = 200\text{--}300$  in 2007–2008,  $\gamma_b = 700\text{--}800$  in 2009–2010), we obtain both an increase of the EC(Disk) component (and the shift of the peak of its emission to higher frequencies), and a simultaneous increase of the SSC. The net result is a roughly achromatic increase of the X-ray emission.

We thank the Referee for useful comments. We thank A. P. Marscher and S. G. Jorstad

---

<sup>6</sup>If considering also the contribution of relativistic protons, with  $\langle\gamma\rangle = 10^2$ , we obtain  $P_{\text{jet}} \approx 10^{49}$  erg s<sup>-1</sup>.

for Perkins and Liverpool Telescopes optical data. We acknowledge financial contribution from: agreement ASI-INAF I/009/10/0, ASI contract I/089/06/2, RFBR Foundation grant 09-02-00092, MICIIN grant AYA2010-14844, CEIC grant P09-FQM-4784, NSF grant AST-0907893, NASA Fermi GI grants NNX08AV65G and NNX10AU15G, NSF/REU grant AST-0851892, the Nantucket Maria Mitchell Association, and grant GNSF/ST08/4-404.

*Facilities:* AGILE, INTEGRAL, *Swift*, WEBT, AAVSO, SMA.

## REFERENCES

- Abdo, A. A. et al. 2011, ApJ, 733, L26
- . 2009, ApJ, 699, 817
- Atwood, W. B. et al. 2009, ApJ, 697, 1071
- Barkov, M. V., Aharonian, F. A., & Bosch-Ramon, V. 2010, ApJ, 724, 1517
- Becker, J. K. 2008, Phys. Rep., 458, 173
- Bonning, E. W. et al. 2009, ApJ, 697, L81
- Bonnoli, G., Ghisellini, G., Foschini, L., Tavecchio, F., & Ghirlanda, G. 2011, MNRAS, 410, 368
- Celotti, A., & Ghisellini, G. 2008, MNRAS, 385, 283
- Chatterjee, R., Baily, C., Bonning, E. W., Buxton, M., Coppi, P., Isler, J., & Urry, C. M. 2011, ApJ, in press, ArXiv:1101.3815
- Courvoisier, T. J.-L. et al. 2003, Astronomy and Astrophysics, 411, L53
- Donnarumma, I. et al. 2010, PoS(INTEGRAL 2010)008
- Finke, J. D., & Dermer, C. D. 2010, ApJ, 714, L303
- Foschini, L., Ghisellini, G., Tavecchio, F., Bonnoli, G., & Stamerra, A. 2011, ArXiv e-prints
- Foschini, L., Tagliaferri, G., Ghisellini, G., Ghirlanda, G., Tavecchio, F., & Bonnoli, G. 2010, MNRAS, 408, 448
- Ghisellini, G., & Celotti, A. 2001, MNRAS, 327, 739
- Ghisellini, G., Foschini, L., Tavecchio, F., & Pian, E. 2007, MNRAS, 382, L82



- Giuliani, A., Chen, A., Mereghetti, S., Pellizzoni, A., Tavani, M., & Vercellone, S. 2004, *Mem. SAIIt Suppl.*, 5, 135
- Gurwell, M. A., Peck, A. B., Hostler, S. R., Darrah, M. R., & Katz, C. A. 2007, in *Astronomical Society of the Pacific Conference Series*, Vol. 375, *From Z-Machines to ALMA: (Sub)Millimeter Spectroscopy of Galaxies*, ed. A. J. Baker, J. Glenn, A. I. Harris, J. G. Mangum, & M. S. Yun, 234
- Jorstad, S. G. et al. 2010, *ApJ*, 715, 362
- Krajci, T., Sokolovsky, K., & Henden, A. 2010, *The Astronomer’s Telegram*, 3047, 1
- Mannheim, K., & Schlickeiser, R. 1994, *A&A*, 286, 983
- Mücke, A., & Protheroe, R. J. 2001, *Astroparticle Physics*, 15, 121
- Pacciani, L. et al. 2010, *ApJ*, 716, L170
- Pian, E. et al. 2010, *The Astronomer’s Telegram*, 3055, 1
- . 2006, *A&A*, 449, L21
- Pittori, C. et al. 2009, *A&A*, 506, 1563
- Poole, T. S. et al. 2008, *MNRAS*, 383, 627
- Raiteri, C. M. et al. 2008a, *A&A*, 485, L17
- . 2008b, *A&A*, 491, 755
- . 2007, *A&A*, 473, 819
- . 2011, *A&A*, Submitted
- Striani, E. et al. 2010a, *The Astronomer’s Telegram*, 3034, 1
- . 2010b, *The Astronomer’s Telegram*, 3043, 1
- . 2010c, *The Astronomer’s Telegram*, 3049, 1
- . 2010d, *ApJ*, 718, 455
- Tavani, M. et al. 2009, *A&A*, 502, 995
- Vercellone, S. et al. 2009, *ApJ*, 690, 1018

- . 2010a, ApJ, 712, 405
- . 2010b, The Astronomer’s Telegram, 2995, 1
- Villata, M. et al. 2007, A&A, 464, L5
- . 2006, A&A, 453, 817
- . 2009, A&A, 504, L9
- . 2008, A&A, 481, L79
- Vittorini, V. et al. 2009, ApJ, 706, 1433